Nano-mechanical properties of silver-welded YBCO bulks

2010 J. Phys.: Conf. Ser. 234 012034

(http://iopscience.iop.org/1742-6596/234/1/012034)

Journal of Physics: Conference Series **234** (2010) 012034 doi:10.1088/1742-6596/234/1/012034

Nano-mechanical properties of silver-welded YBCO bulks

J J Roa[1], E. Bartolomé[2], B. Bozzo[3], X. G. Capdevila[1], X. Granados[3], M. Segarra[1]

[1] Department of Materials Science and Metallurgical Engineering, University of Barcelona; 08028 Barcelona (Spain)
[2] Escola Universitaria Salesiana de Sarrià (associated to the University Autònoma of Barcelona), Passeig Sant Joan Bosco 74, 08017 Barcelona (Spain)
[3] Institut de Ciència de Materials de Barcelona–CSIC; Campus UAB; 08193 Bellaterra (Spain)

E-mail: joanjosep_roa@ub.edu

Abstract. The mechanical properties of melt-textured YBCO bulk boundaries are a topic of special interest especially in the manufacturing of superconductor devices for engineering applications. Instrumented indentation technique is a powerful tool widely employed to characterize the mechanical properties of small volumes. We presented results of the nanohardness (H) and Young's modulus (E) across [001]-welds fabricated by silver welding. The residual imprints performed by a sharp tip indenter were observed by Field Emission Scanning Electron Microscope (FE-SEM) to investigate the different fracture mechanisms nucleated during the indentation process. Results show a decrease of the nanohardness across the grain boundary related to the appearance of a "welding path" free of Y-211 particles. The FE-SEM images show chipping and sink-in effects in that region. Remarkably, for zero-angle welds the mechanical properties are unaltered across the joint, thus probing the high quality of silver welds for large-scale applications.

1. Introduction

High-T_c bulk superconductor materials exhibit high critical current densities (J_c), and can thus trap high magnetic fields. However, melt-texture YBCO presents poor mechanical properties, so that the mechanical strength is extremely low compared with structural ceramics [1]. In the last decade, the silver welding technique consisting in joining two single domains bulk superconductors with an agent having lower peritectic temperature (i.e. silver foil), has emerged as one of the most promising techniques to obtain large size bulks. While the magnetic properties of silver welds have been thoroughly investigated [2], the mechanical properties such as the hardness (H), Young's modulus (E), toughness fracture (K_{IC}), should be known for the industrial applications [2].

Nanoindentation or depth-sensing instrumented indentation is nowadays a useful technique for the mechanical characterization of materials in a wide range of scales, from few nanometres to micron and millimetre range. In a nanoindentation test, a diamond indenter of known geometry is pressed into a material, and the penetration depth (h), is constantly recorded against the applied load (P) during a loading and the unloading cycle [3, 4]. Figure 1 shows a typical P-h curve after five load-unload processes. The unloading curve is associated to a pure elastic deformation, while the loading curve is associated to an elasto-to-plastic deformation mechanism. The analysis of the P-h curves allows the experimental determination of the Young's modulus, E, and the nanohardness, H.

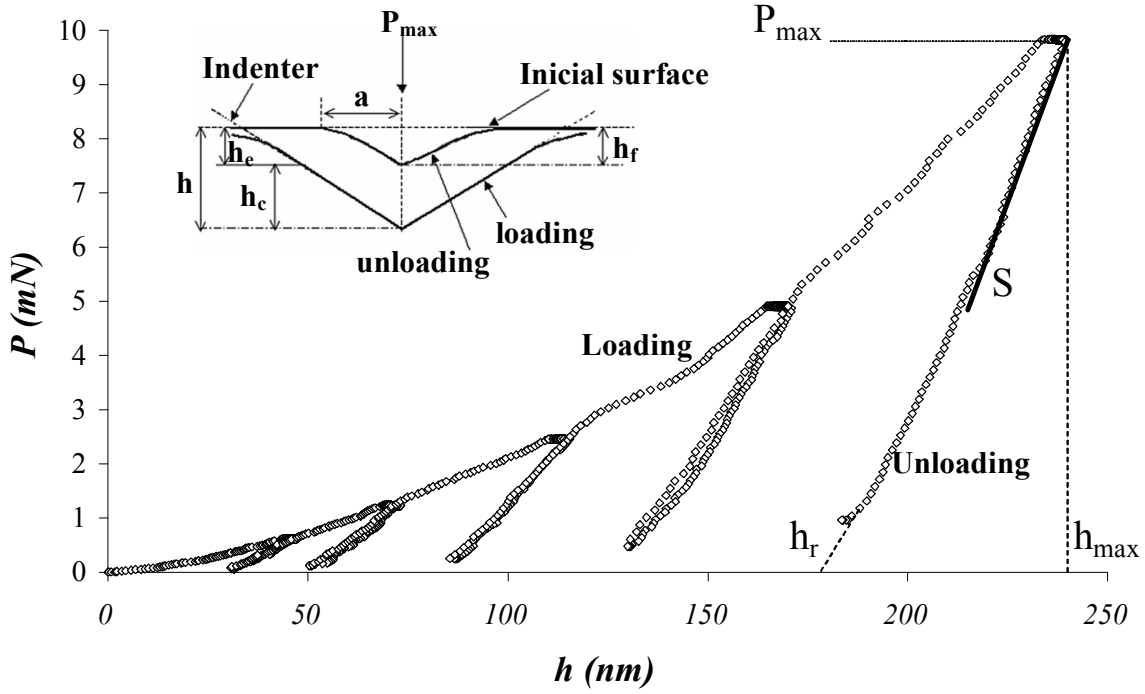

Figure 1. Typical load (P) versus penetration depth (h) curve of load-unload instrumented indentation test, the maximum applied load (P_{max}), maximum penetration depth (h_{max} or h), residual depth (h_r), the contact penetration depth (h_c), the elastic penetration depth (h_e), the contact point between sample and indenter (a) and Stiffness (S) can be appreciated.

In this paper, we have investigated the mechanical properties of melt-textured YBCO silver welds using the nanoindentation technique at 10 mN of maximum applied load. Moreover, the different fracture mechanisms nucleated during the indentation process have been visualized by Field-Emission Scanning Electron Microscopy (FE-SEM) in order to understand the plastic behaviour taking place.

2. Sample preparation

We studied two welds with [001]-tilt misorientation θ=0º and 14º angles, prepared using the silver welding methodology [5, 6]. The method consists basically of assembling a metallic 10 μm thick Ag foil in between the two misoriented melt-textured, commercial YBCO tiles joined in a sandwich-like configuration. The specimen is then first heated up to T_{max}=995ºC and dwelt for 3 hours; then it follows a slow-cooling rate from 980ºC down to 950ºC and last it is fast-cooled to room temperature. Finally, the welded sample is annealed in flowing oxygen at 1.1bar for 120 hours at 450ºC. The actual misorientation angle was determined from the observation of the twin plane families at both sides of the boundary on an *ab*-plane with the help of an optical microscope with polarized light. The inter-to-intragrain critical current density ratios determined in the past from quantitative magnetic Hall scanning microscopy were $J_c^{GB}/J_c^{G}(\theta=0º)=1$ and $J_c^{GB}/J_c^{G}(\theta=14º)=0.78$.

3. Mechanical characterization

We used the method developed by Oliver and Pharr [8, 9] to determine the hardness (H) and the elastic modulus (E) from the unloading part of recorded indentation P-h curves, such as Fig.1. The H is calculated by dividing the load by the projected contact area A_c at maximum applied load P_{max}:

$$H = \frac{P_{\max}}{A(h_c)}, \qquad (1)$$

where the parameter h_c is determined as:

$$h_c = h_{\max} - \varepsilon \frac{P_{\max}}{S}, \quad (2)$$

being h_{max} the maximum penetration depth, ε a parameter approximately equal to 0.75 for a Berkovich indenter, and S the unloading contact stiffness at maximum penetration depth (see *Fig. 1*). In the case of a perfect Berkovich tip, $A=24.56h_c^2$. However, in practice the projected contact area differs from this value when the tip is worn out, because the different faces angles may be somehow different from the nominal. Hence, the projected contact area must be calibrated every month. When catastrophic fracture mechanisms occur, the A_c obtained by this theoretical method is overestimated and results in an H underestimation. To avoid this problem, we experimentally determined the real contact area A_c from FE-SEM images of the residual imprints.

The effective elastic modulus (E_{eff}) has been expressed in terms of S and A_c as:

$$E_{eff} = \frac{1}{\beta}\frac{\sqrt{\pi}}{2}\frac{S}{\sqrt{A(h_c)}}, \quad (3)$$

where β is a geometrical factor (1.034). This parameter takes into account the lack of symmetry of the Berkovich indenter, as equations 1-3 are developed for an axisymmetric indenter.

Then, according to the Oliver and Pharr approach [8], the Young's modulus can be obtained as:

$$\frac{1}{E_{eff}} = \frac{1-\nu^2}{E} + \frac{1-\nu_i^2}{E_i}, \quad (4)$$

where E and ν are the Young's modulus and the Poisson's ratio (υ_{YBCO}=0.3 [10]), respectively. The subindex i denotes the indenter properties (E_i=1141 GPa and ν_i=0.07 [8]).

In order to investigate the variation of the mechanical properties across the welding zone, a series of nanoindentations have been performed on the *ab*-plane in a range of 2000 mm across the boundary at 10 mN of maximum applied load. The separation between imprints was 50 μm in order to isolate the plastic behaviour created during the indentation process by the Berkovich imprint. Six hundred indentations were performed for each sample in order to achieve statistical significance. Each of the H data points plotted in subsequent images is the average of 15 scans performed across the welding zone.

4. Results and Discussion

4.1. Mechanical properties

The mechanical properties across two silver YBCO welds with Θ=0º and 14º misorientation angles in the orthorhombic phase have been obtained with the Oliver and Pharr method [9]. The Young's modulus for each studied sample was E=120 ± 5 GPa, without degradation at the weld region. This should be expected, as this parameter is an intrinsic material YBCO property. This value is in agreement with reported values for YBCO Bridgman samples in the literature obtained with other techniques (i.e. bending [10], spherical indentation [11], X-ray diffraction [12]).

Figure 2 shows the H evolution across the welding zone for Θ=0º and 14º angle welds in orthorhombic phase. Notably, the sample with a 0º misorientation displays no reduction of H across the weld. A microstructure analysis (Fig. 2, inset) reveals that the density of Y-211 particles vanishes in a welding path of approximately the same width. The existence of this zone in silver welds has been explained by the higher Y content in the melt produced by diffusion and dissolving of solid bulk phases in melted Ag during the thermal treatment [13]. The nanohardness of the Y-211 phase is almost a factor of two large than that of the Y-123 phase, as concluded from nanoindentation measurements at the same applied loads [10]. Due to the absence of Y-211 particles near the welding zone, a reduction of the YBCO compound hardness take place.

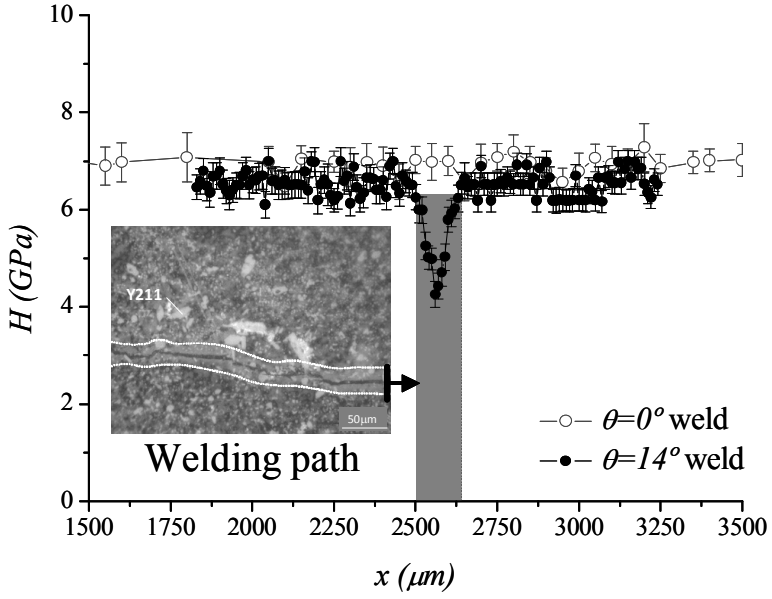

Figure 2. Nanohardness scans, *H(x),* across Θ=0º and 14º weld for the orthorrombic phase.

4.2. Fracture mechanisms

The high stress concentrated under the contact point between sample and indenter during the indentation process nucleates different fracture mechanisms. When the stress nucleated by the sharp indenter exceeds a limiting value, sink-in, chipping mechanism and crack propagation at the corners of the residual imprint are induced.

We investigated by FE-SEM the residual imprints of silver welds to obtain information about the plastic behaviour taking place during the indentation process. Figure 3a and b shows the residual nanoindentation imprints for θ=0º weld performed outside and inside the welding zone, respectively. A little pore density is nucleated near the imprint. These imprints exhibit microcracks at the corners of the residual imprint typically observed in ceramics. Figure 3c and d shows in contrast residual nanoimprints outside and inside the weld region for the θ=14º weld. Outside the welding zone, the fracture mechanisms are similar to those observed for θ=0º sample (Fig. 3c). However, imprints performed in the welding zone show sink-in and chipping effects due to the field stress generated around the imprint.

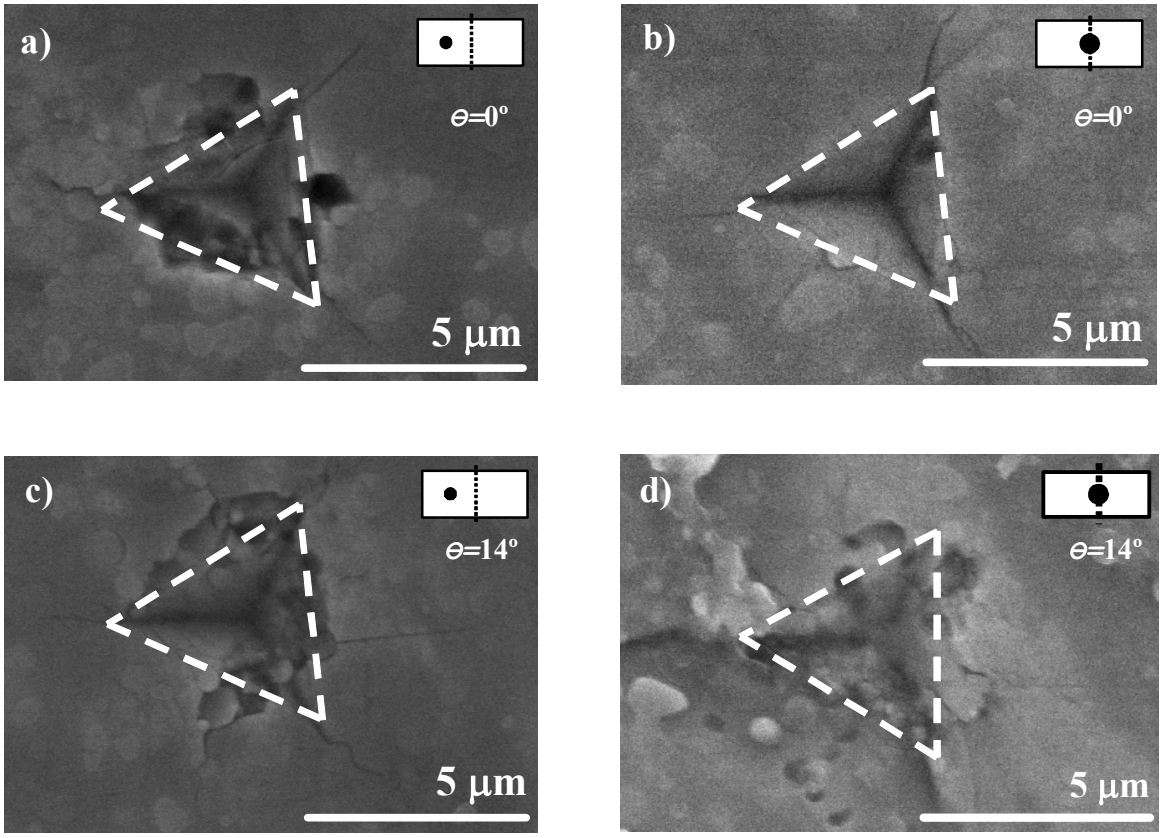

Figure 3. Residual nanoindentation imprints in melt-textured YBCO samples obtained by FE-SEM and performed at 10 mN of applied load in the *ab*-plane ***a)*** outside of θ=0º welding zone, ***b)*** *at* θ=0º weld region, ***c)*** outside of θ=14º welding zone, and ***d)*** *at* θ=14º weld.

5. Conclusions

Nanoindentation has proved to be a powerful technique for the mechanical characterization of superconducting welds. The Young's modulus and nanohardness of different [001]-tilt misoriented YBCO welds grown by the silver welding technique were experimentally obtained. The Young's modulus was E=120±5 GPa, for all the samples, without degradation at the weld region. This value is in agreement with values reported in bibliography obtained by different techniques. A decrease in the nanohardness H has been measured for misoriented welds, correlated with the absence of Y211 hard particles in a *welding-path* of a width of 50 μm around the boundary. Sinking and chipping fracture mechanisms induced by the indentation process occur in that region. Notably, for high quality 0º-welds with inter-to-intragrain critical current density ratio J_c^{GB}/J_c^{G}=1, the nanohardness is constant across the boundary, and the nanoimprints inside and outside the welding zone present similar aspect, free of catastrophic fracture mechanisms. Thus, we have shown that high quality 0º-welds with optimal magnetic and mechanical characteristics can be fabricated by the silver welding technique. This paves the path for bulk applications requiring large pieces.

6. Acknowledgments

The authors would like to thank the Serveis Cientificotècnics (SCT, University of Barcelona) for the FE-SEM data. Also, we would like to thank W. Boch from NEXANS Superconductors for providing the bulk materials. J. J. Roa thanks the finantial support from the "*Comissionat per la Universitat i la Investigació del Departament d'innovació Universitari i d'Empresa de la Generalitat de Catalunya i el Fons Social Europeu* ". E. Bartolomé thanks the financial support from MEC (No. MAT2005-

02047), Generalitat de Catalunya (XaRMAE and Pla de Recerca SGR-0029) and EU (No. HIPERCHEM-STREP 516858 and NESPA European Project) and Nanoselect CONSOLIDER Project (No. CSD2007-00041).

7. References

[1] Nishida A, Terai K, and Hatanaka K 1993 *J. Soc. Mat. Sci.* **42** 426.
[2] Bartolome E *et al* 2008 *Supercond. Sci. Technol.* **21** 12502.
[3] Jiménez-Piqué E, Gaillard Y, and Anglada M 2007 *Key Eng. Mater.* **333** 107.
[4] Chinh N Q, Gubicza J, Kovács Zs, and Lendvai J 2003 *J. Mater. Res.* **19** 31.
[5] Walter H, Jooss C, Sandiumenge F, Bringmann B, Delamare M P, Leenders A, and Freyhardt H C 2001 *Europhys. Lett.* **55** 100.
[6] Iliescu S, Granados X, Bartolomé E, Sena S, Carrillo A E, Puig T, Obradors X, and Evetts J E 2004 *Supercond. Sci. Technol.* **17** 182.
[7] Pharr G M 1998 *Mat. Sci. Eng. A* **253** 151.
[8] Pharr G M, Oliver W C, and Brotzen F R 1992 *J. Mater. Res.* **7** 613.
[9] Oliver W C, and Pharr G M 1992 *J. Mater. Res.* **7** 1564.
[10] Roa J J, Capdevila X G, Martínez M, Espiell F, and Segarra M 2007 *Nanotechnology* **18** 385701.
[11] Roa J J, Jiménez-Piqué E, Capdevila X G, and Segarra M 2009 *J. Eur. Ceram. Soc.* Submitted.
[12] Block S, Piermarini G J, Munro R G, and Wong-Ng W 1987 *Adv. Ceram. Mater.* **2** 601.
[13] Sefcikova M *et al* 2008 *Mat. Sci. Eng. B* **151** 107.
[14] Tancret F, Monot I, and Osterstock F 2001 *Sci. Eng. A.* **298** 268.
[15] Sakai N, Seo S J, Inoure K, Miyamoto T, and Murakami M 2000 *Physica C* **335** 107.